THE JOURNAL OF PHYSICAL CHEMISTRY C

Article

pubs.acs.org/JPCC

Facile Synthesis and Evaluation of Nanofibrous Iron–Carbon Based Non-Precious Oxygen Reduction Reaction Catalysts for Li–O_2 Battery Applications

Jason Wu, Hey Woong Park, Aiping Yu, Drew Higgins, and Zhongwei Chen*

Department of Chemical Engineering, Waterloo Institute for Nanotechnology, Waterloo Institute for Sustainable Energy, University of Waterloo, Waterloo, Ontario, Canada, N2L 3G1

Supporting Information

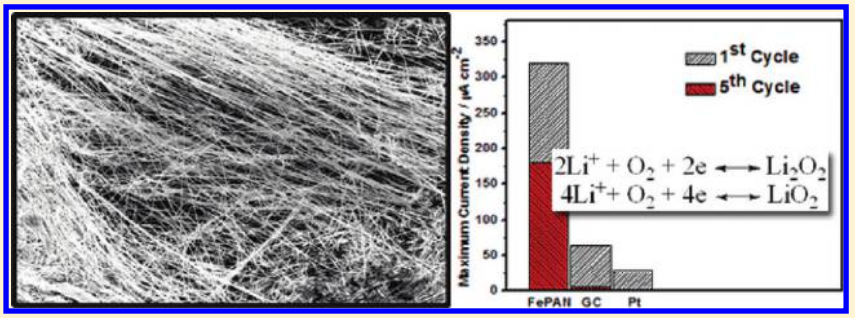

ABSTRACT: Development of low cost active catalysts toward oxygen reduction reaction (ORR) is critical for the effective operation of Li–O_2 battery. Porous nonprecious iron–carbon based nanofiber catalysts have been developed by electrospinning method. The catalysts demonstrated similar ORR catalytic activity for ORR as the commercial Pt-based catalysts in the aqueous half-cell voltammetry sweeps. In the Li–O_2 aprotic environment, the catalyst exhibited higher on-set potentials when compared to glassy carbon and Pt disk electrodes. The results show that the nonprecious electrospun nanofiber could be an effective low cost ORR catalyst at the cathode for Li–O_2 battery.

INTRODUCTION

The use of conventional lithium-ion batteries in electric vehicle applications are limited by their insufficient gravimetric energy and power density, stemming primarily from the poor cathodic Li ion intercalation.[1−3] Optimization of this technology using currently available materials are only projected to improve the energy density of the battery by 50%, which is insufficient for the high energy demands of electric automotive vehicles.[3] An alternative approach in battery technology that has shown promise is the replacement of the intercalation material at the cathode with a catalytically active oxygen reduction reaction (ORR) electrode. These batteries, dubbed as lithium–oxygen (Li–O_2) batteries, possess the potential to provide three to five times the energy density of conventional Li-ion batteries.[3−6] The discharge reaction varies between the different types of Li–O_2 chemical architectures currently pursued. Three of the chemical architectures are liquid based, including: (1) aprotic, (2) aqueous, and (3) mixed aqueous/aprotic, whereas the fourth type is completely (4) solid state.[7] In an aprotic Li–O_2 battery, the discharge reaction involves a $2e^-$ transfer process resulting in the formation of lithium peroxide (1) or lithium oxide (2) at the cathode.[3−5,7,8] The battery is regenerated during charging, which results in the decomposition of lithium peroxide/oxide to form lithium and oxygen.[3−5,7,8]

$$2Li^+ + O_2 + 2e \leftrightarrow Li_2O_2 \quad (1)$$

$$4Li^+ + O_2 + 4e \leftrightarrow 2Li_2O \quad (2)$$

The fundamental discharge reactions are shown above and occur at nearly identical potentials (E_{rev} = 2.96 V vs Li and E_{rev} = 2.91 V vs Li, respectively).[3−5,7−9] They are both thermodynamically favorable, and heavily influenced by ORR kinetics.

A number of issues prevent the practical widespread use of Li–O_2 batteries, including poor rate capability, poor round-trip efficiency, and poor cycle life.[4,5,10] These issues are a direct result of poor discharge performance due to high cathodic overpotentials and slow ORR kinetics.[4,5] Poor discharge performance results in low deliverable gravimetric energy and power densities of the battery. It is critical to use electrocatalysts for ORR as part of the cathode material to enhance ORR kinetics, lower overpotentials, and thus improve the discharge performance. Additionally, the cathode material must possess high surface area as well as the capability to allow the formation of the insoluble discharge reaction products.

Platinum-based electrocatalysts are known to exhibit high activity toward ORR.[8,11−13] These electrocatalysts are commonly used in fuel cells to expedite the slow ORR kinetics at

Received: February 19, 2012
Revised: March 29, 2012
Published: April 14, 2012

dx.doi.org/10.1021/jp301644e | J. Phys. Chem. C 2012, 116, 9427−9432

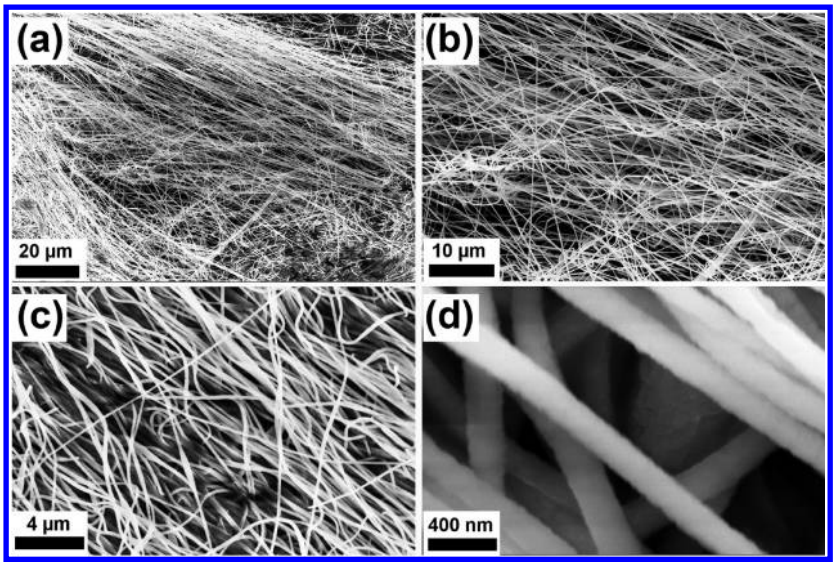

Figure 1. Scanning electron micrographs of electrospun polyacrylonitrile nanofibers containing iron acetate prior to preoxidation and carbonization heat treatments. Image taken at (a) 1000×, (b) 2000×, (c) 5000×, and (d) 50 000× magnification.

the cathode and can be considered applicable to Li−O_2 batteries. However, there is a significant disadvantage of using precious metal catalysts such as Pt due to the high cost of the metal. Nonprecious carbon-based catalysts for ORR are promising candidates in replacing the expensive Pt metal catalysts.[6,11,14−25] As these catalysts operate in alkaline conditions where the performance of the catalysts may even exceed Pt catalysts,[20,25] it is possible to forego the use of the precious metal and replace Pt with nonprecious alternatives.

For a nonprecious catalyst to be considered, it must possess (a) high activity in alkaline conditions, and (b) allow for the formation of the discharge reaction products. In the present work, an iron−carbon based nonprecious electrocatalyst for ORR is synthesized via electrospinning to produce a mat of anisotropic 1D porous nanofibers. The ORR activity of these materials is on par with Pt/C-based catalysts in an aqueous alkaline environment. With the aqueous ORR activity of the nonprecious catalyst proven, the primary focus of the present work is to evaluate the nonprecious catalyst for its aprotic Li−O_2 ORR activity. As the catalyst is carbon based, the catalyst is also capable of doubling as a platform for the formation of lithium (per)oxide. These nanofibers are produced via electrospinning technique, which allows for the facile synthesis of nanofiber or nanowire structured materials. Synthesis of the nonprecious nanofibrous catalyst begins with electrospinning a solution of polyacrylonitrile (PAN) and iron acetate. PAN naturally forms into carbon fibers after heat treatment at high temperatures in an inert atmosphere,[26] creating highly conductive, 1D structures that can be arranged into porous electrode structures with excellent mass transport properties. Furthermore, PAN possesses thermally stable nitrogen species,[26] which are essential in forming active nonprecious catalysts after pyrolysis with an iron salt. After pyrolysis (FePAN-PL), the nonprecious nanofibrous catalyst is acid leached to remove excess iron particles that have agglomerated during the heat treatment process. This is followed by a second pyrolysis in Ar gas (FePAN) resulting in highly active, porous FePAN nanofibrous catalysts. The final FePAN nanofibrous catalyst is electrochemically characterized via RDE technique in an aqueous and, for the first time, an aprotic environment. The aprotic ORR performance is evaluated by comparing the FePAN nanofibrous catalyst with a bare glassy carbon and Pt disk electrode. Further characterization involving both the physicochemical properties of the FePAN nanofibrous catalyst is conducted via SEM, TEM, and XPS analysis.

EXPERIMENTAL SECTION

Synthesis of FePAN-PL Nanofibrous Catalyst. Preparation of preacid leached FePAN carbon nanofibers begins by electrospinning a solution of 5 wt % PAN in DMF along with 0.2 wt % of iron from iron acetate. The solution is electrospun at a distance of 13 cm between the tip of the needle and a grounded collector with an applied potential of 13 kV. The nanofibers are collected, dried, and preoxidized at 250 °C for 3 h in air before being carbonized at 900 °C for 30 min in Ar gas.

Synthesis of FePAN Nanofibrous Catalyst. FePAN-PL is taken and treated with 0.5 M sulfuric acid at 80 °C for 24 h to remove surface iron particles. The FePAN nanofibrous catalyst is filtrated, thoroughly washed, and dried overnight before entering a second pyrolysis at 900 °C in Ar for 30 min.

Electrochemical Characterization. Electrochemical characterization of the FePAN nanofibrous catalyst was carried out via RDE technique, first by preparing a catalyst ink with a concentration of 2 mg/mL. The ink was then deposited onto a glassy carbon electrode 8 uL at a time for five times before applying 8 uL of 0.5 wt % Nafion solution. Linear sweep curves were obtained for the FePAN nanofibrous catalyst at 100 rpm, 400 rpm, 900 rpm, and 1600 rpm in O_2 saturated 0.1 M KOH and corrected for the background current. The background current was obtained by saturating the 0.1 M KOH electrolyte in N_2 gas and obtaining a linear sweep scan. The Li−O_2 performance in aprotic solutions is carried out in an air-sealed three-necked flask using a solution of $LiPF_6$ in tetraethylene glycol dimethyl ether (TEGDME) as the aprotic electrolyte and Li metal as the counter and reference electrode. The results are also corrected for the background current by obtaining a linear sweep scan of the FePAN nnaofibrous catalyst in Ar-saturated TEGDME electrolyte.

Catalyst Characterization. Morphology of the FePAN nanofibrous catalyst was analyzed via SEM and TEM imaging. TEM samples were prepared by dispersing the catalyst in

dx.doi.org/10.1021/jp301644e | J. Phys. Chem. C 2012, 116, 9427−9432

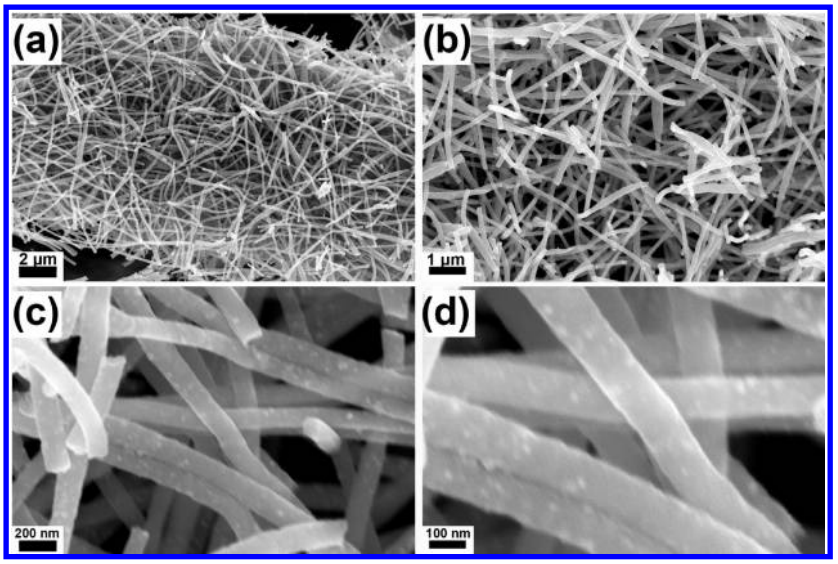

Figure 2. Scanning electron micrographs of FePAN4-PL nanofibrous catalyst at (a) 5000×, (b) 10 000×, (c) 50 000×, and (d) 100 000× magnification.

methanol before applying a droplet of the dispersed catalyst onto a copper grid. The surface areas of the FePAN nanofibrous catalysts are determined via BET analysis. Samples were degassed at a temperature of 250 °C for 12 h before obtaining the Nitrogen adsorption isotherm. XPS analysis was conducted on the N 1s, C 1s, and Fe 2p lines for the catalyst at a takeoff angle of 90° using an Al Kα X-ray source with a spot area of 400 μm.

RESULTS AND DISCUSSION

The electrospun PAN nanofibers containing iron acetate are shown in Figure 1. The nanofibers are arranged in a mesh with diameters of 100−200 nm. The nanofibers retain their diameter after preoxidation and carbonization. From Figure 2, it is possible to see that the pyrolyzed iron containing FePAN nanofibrous catalysts remain in a mesh with ample space between each fiber, allowing for excellent mass transport properties. The SEM images also indicate the presence of small iron particles both at the surface and embedded within the carbon nanofibers. TEM images in parts a and c of Figure 3 shows the rough surface morphology of the nanofibers after the first pyrolysis (FePAN-PL). The same images confirm the presence of iron particles, roughly 20 nm in diameter, that are on the surface and embedded within a layer of carbon. Furthermore, the surface roughness of the nanofibers near the iron particles hints that the fibers may contain a porous structure after the high temperature treatment. It is possible that the iron metal could catalyze carbonization of the fibers, causing localized weight loss, and the resulting rapid release of gaseous species[26] would result in the creation of porous carbon nanofibers. A second pyrolysis after treating the fibers in 0.5 M H_2SO_4 at 80 °C resulted in much rougher surfaces as seen in parts b and c of Figure 3 (FePAN). It is also possible to see the emergence of many more iron particles on the surface of the fibers, likely due to additional weight loss of the carbon material during the second pyrolysis. The surface roughness and empty carbon shell-like structures seen on the surface of the nanofibers further suggest that the acid leached catalyst is porous. As the surface area of the fibers directly impacts both the ORR kinetics (through mass transport) and the discharge

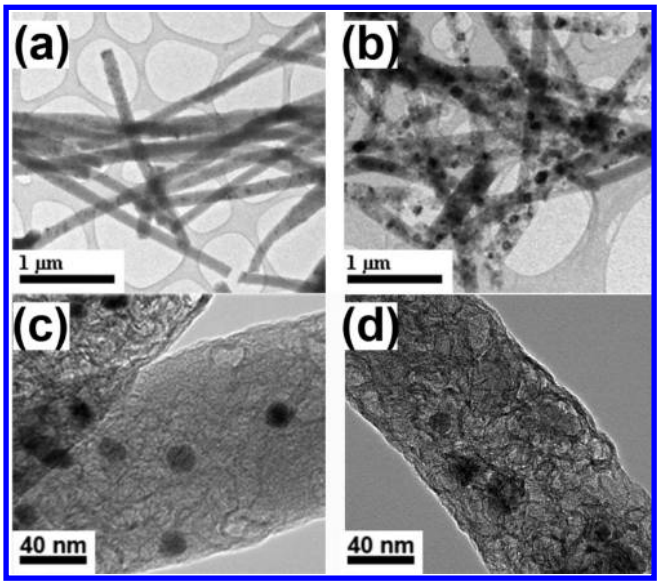

Figure 3. Transmission electron micrographs of (a, c) FePAN-PL, and (b, d) FePAN nanofibrous catalysts.

current (in forming Li_2O_2 or Li_2O), the production of porous nanofibers is an added benefit as it allows for more exposed ORR active sites as well as surface carbon sites for the formation of the discharge reaction products. To confirm the surface areas of the two samples, the BET surface areas were obtained from their respective nitrogen adsorption isotherms. A significant increase in surface area from 82.4447 $m^2\ g^{-1}$ to 339.1079 $m^2\ g^{-1}$ is found after acid leeching and repryolysis of the fibers. The result suggests that the acid leeched and repyrolyzed fibers should provide improved ORR performance in both aqueous and aprotic conditions.

The half-cell ORR performance of the single pyrolyzed, preacid leached (FePAN-PL) and double pyrolyzed (FePAN) iron−carbon nanofibrous catalysts are shown in Figure 4. The benefits of higher surface area and porosity are immediately seen as the double pyrolyzed catalyst exhibits dramatically increased current densities over its single pyrolyzed prede-cessor. Without acid treatment and a second pyrolysis, the

dx.doi.org/10.1021/jp301644e | J. Phys. Chem. C 2012, 116, 9427−9432

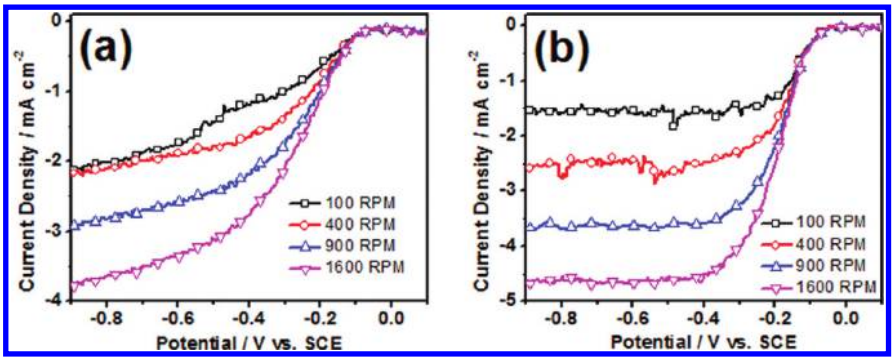

Figure 4. ORR polarization curves in aqueous 0.1 KOH for (a) FePAN-PL, and (b) FePAN nanofibrous catalysts.

FePAN nanofibrous catalyst exhibits lower limiting currents and poor limiting current characteristics. After acid treatment and subsequent second pryolysis, the FePAN nanofibrous catalyst exhibits a high limiting current that plateaus quickly. The on-set potentials of both FePAN nanofibrous catalysts remain the same, suggesting that the type of active site formed during pyrolysis of the catalysts is not changed after acid treatment and a second pyrolysis. In this case, the acid treatment and second pyrolysis of the samples is a purely physical modification of the catalyst, and does not alter the active sites. This assumption is supported by the examination of the electronic structure of the elements of the two catalysts. A comparison of the N 1s XPS spectra, often associated with discussions of the ORR active site, can be seen in parts a and b

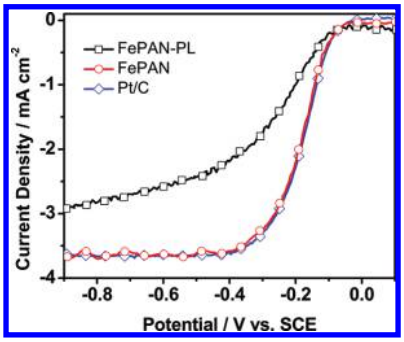

Figure 5. Comparison of ORR activity in aqueous 0.1 M KOH at 900 rpm of FePAN-PL nanofibrous catalyst, FePAN nanofibrous catalyst, and Pt/C catalyst.

of Figure 6, for FePAN-PL and FePAN, respectively. No difference in the two spectra can be observed with both catalysts containing the majority of the surface nitrogen in the pyridinic (398.08 eV) and graphitic (400.88 eV)[14,27,28] binding state. An analysis of the Fe 2p, C 1s, and O 1s spectra with fitted peaks are also shown in Figure 6. The Fe 2p spectra (parts c and d of Figure 6) also show no differences in the electronic structure of iron within the two catalysts. Additionally, the Fe 2p spectra indicate that the majority of the surface iron within the two catalysts exists in an ionic state.[14,27] It is possible that the surface iron could exist as oxidized iron, nitrogen bound iron, or hydroxide bound iron. The C 1s spectra of the two catalysts exhibit large peaks at 284.8 eV, indicating that the catalysts contain large quantities of sp2-hybridized carbon,[27] followed by the next highest peaks at 285.7 eV, indicating nitrogen−carbon binding types.[27]

The high ORR activity of the FePAN nanofibrous catalyst in an aqueous alkaline environment is confirmed by comparing its performance to a commercially available Pt/C catalyst (Figure 5). In comparison with Pt in an aqueous environment it can be seen that the ORR activity, on-set and limiting currents, are comparable. The limiting current achieved by the nonprecious FePAN nanofibrous catalyst is on par with that of the precious metal, thus significant reduction in catalyst cost can be achieved by employing nonprecious catalysts without performance loss. With this in mind, it is possible to utilize nonprecious carbon catalysts exhibiting superior ORR kinetics without the need to employ expensive Pt catalysts. Furthermore, as the ORR catalyst is carbon based, no additional carbon support is required for the formation of lithium peroxide.

The Li−O_2 cell performance of the nonprecious FePAN nanofibrous catalyst in aprotic solutions is shown in Figure 7. The aprotic solution is O_2-saturated and the glassy carbon electrode coated with the catalyst ink is scanned from 2.0 to 4.3 V versus Li/Li+ at a scan rate of 5 mV s^{-1}. The FePAN nanofibrous catalyst-coated electrode is then compared with a bare glassy carbon electrode and a Pt disk electrode. Figure S3 of the Supporting Information shows the cyclic voltammogram of the FePAN nanofibrous catalyst in both Ar- and O_2-saturated electrolytes. From the scan, it is possible to see that no electrochemical reactions are taking place without the presence of oxygen, indicating that the catalyst does not react with the aprotic electrolyte.[29] The standard potential for the ORR/OER reactions are known to occur at 2.96 V vs Li/Li+ for a two electron process, resulting in the formation of lithium peroxide ($2Li + O_2 \rightarrow Li_2O_2$) for the ORR, and the formation of lithium ions and oxygen ($Li_2O_2 \rightarrow 2Li + O_2$) for the OER. Both the ORR and OER processes are shown to occur in the O_2-saturated curve in Figure S3 of the Supporting Information for the FePAN nanofibrous catalyst. In Figure S3 of the Supporting Information, anodic peaks in the O_2-saturated curve are observed indicating the formation of the discharge products when in the presence of oxygen (ORR). Once the reversed potential scan approaches roughly 3.3 V vs Li/Li+, cathodic peaks are also observed indicating the decomposition of the discharge products on the surface of the electrode (OER).[29] The FePAN nanofibrous catalyst exhibits higher reduction currents and on-set potentials than both the glassy carbon and Pt disk electrode at all potentials. The superior reduction currents achieved by the catalyst are likely due to the catalyst's significantly higher surface area as a result of the porous network of carbon fibers —allowing for more discharge reaction products to be formed.[7] The reduction on-set potential occurs at a potential closer to 2.96 V versus Li/Li+, for the first cycle, than the on-set potentials of both Pt (2.80 V vs Li/Li+) and the glassy carbon electrode (2.78 V vs Li/Li+) suggesting

dx.doi.org/10.1021/jp301644e | J. Phys. Chem. C 2012, 116, 9427−9432

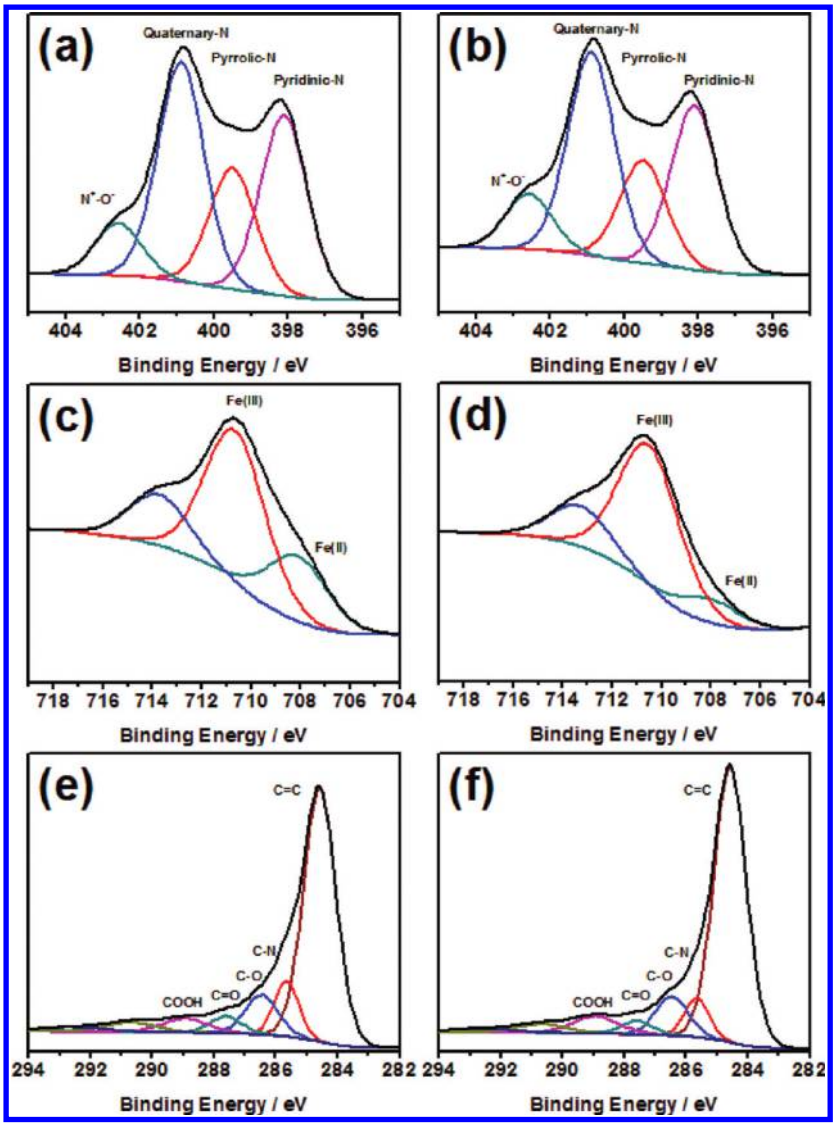

Figure 6. XPS spectra of the (a) N 1s scan of FePAN-PL, (b) N 1s scan of FePAN, (c) Fe 2p scan of FePAN-PL, (d) Fe 2p scan of FePAN, (e) C 1s scan of FePAN-PL, (f) C 1s scan of FePAN nanofibrous catalysts.

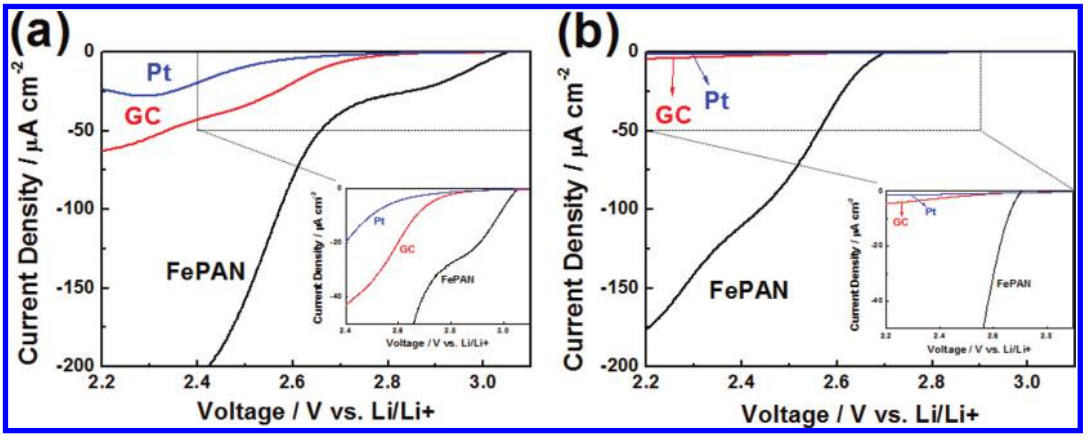

Figure 7. (a) Initial ORR polarization curves of FePAN nnaofibrous catalyst on GC, polycrystalline GC and Pt surfaces in O_2-saturated 1.0 M $LiPF_6$ in TEGDME at 900 rpm and 5 mV s^{-1}; and (b) 5th ORR polarization curves during cycling between 2.0 and 4.3 V.

superior ORR kinetics. Part b of Figure 7 shows the fifth ORR profile during cycling between 2.0 and 4.3 V, where the FePAN nanofibrous catalyst is observed to retain acceptable current density for ORR after multiple charge−discharge cycles. The FePAN nanofibrous catalyst exhibits a maximum current density, occurring at 2.15 V versus Li/Li+, of ca. 320 μA cm^{-2} on the first cycle. The maximum current density achieved by the FePAN nanofibrous catalyst is eleven times greater than

dx.doi.org/10.1021/jp301644e | J. Phys. Chem. C 2012, 116, 9427−9432

the current achieved by the Pt disk electrode (ca. 28 μA cm^{-2}) and five times greater than the current achieved by the glassy carbon electrode (ca. 64 μA cm^{-2}). On the fifth cycle, the catalyst retains 56% of the maximum current density achieved on the first cycle (ca. 180 μA cm^{-2}) also occurring at a potential of 2.15 V versus Li/Li+. Both the Pt disk and glassy carbon electrode exhibit significantly lower retention of their activity after the fifth cycle. The Pt disk electrode retains only 7% of its maximum current density (ca. 28 μA cm^{-2} to 2 μA cm^{-2} in five cycles), and the glassy carbon electrode retains only 9% of its maximum current density (ca. 64 μA cm^{-2} to 6 μA cm^{-2}). The significant difference in activity retention between the FePAN nanofibrous catalyst and the two electrodes could suggest that the nonprecious FePAN nanofibrous catalyst has an additional propensity toward catalyzing OER resulting in the regeneration of active sites. Further studies and improvements to the OER activity of the catalyst as well as improving the surface area of the FePAN nanofibrous catalyst can potentially yield much higher reduction currents and cycle stability.

CONCLUSIONS

The use of a nonprecious iron−carbon-based catalyst for the ORR at the cathode for a Li−O_2 battery is presented and evaluated. The nonprecious FePAN catalyst consists of a mesh of 1D carbon nanofibers containing a porous structure fabricated by electrospinning of a PAN based solution. The addition of an iron salt to the electrospinning solution results in carbon nanofibers with activity toward the ORR, following pyrolysis. Subsequent acid leeching and repyrolysis of the FePAN nanofibrous catalyst induces porosity into the carbon nanofibers, while maintaining the active site, as indicated by both linear sweep voltammetry and the XPS spectra. The added benefit of the increased porosity of the carbon nanofibers results in a higher surface area catalyst with more exposed active sites, resulting in a catalyst that exhibits excellent electrochemical half-cell characteristics with swiftly occurring and high limiting currents. The FePAN nanofibrous catalyst presented is comparable to commercial Pt-based catalysts in term of ORR activity and performance as is shown in the half-cell aqueous linear voltammetry sweeps. In Li−O_2 aprotic environment, the FePAN nanofibrous catalyst exhibited higher on-set potentials when compared to glassy carbon and Pt disk electrodes. From this result, it may be possible to produce cheap and highly effective electrocatalysts to be used as part of the cathode material in a Li−O_2 battery, by synthesizing porous, one-dimensional transition metal containing carbon nanofibers. Further improvements to the porosity of the carbon fibers could produce extremely high surface area catalysts to allow for increased formation of lithium peroxide, which will greatly enhance the discharge current of the material.

ASSOCIATED CONTENT

Supporting Information

EDS spectra, cyclic voltammogram in Ar- and O_2-saturated aprotic electrolyte of the FePAN catalyst. This material is available free of charge via the Internet at http://pubs.acs.org.

AUTHOR INFORMATION

Corresponding Author

*E-mail: zhwchen@uwaterloo.ca.

Notes

The authors declare no competing financial interest.

ACKNOWLEDGMENTS

This work was financially supported by the Natural Sciences and Engineering Research Council of Canada (NSERC), the University of Waterloo and the Waterloo Institute for Nanotechnology.

REFERENCES

(1) Arico, A. S.; Bruce, P.; Scrosati, B.; Tarascon, J.-M.; van Schalkwijk, W. *Nat. Mater.* **2005**, *4*, 366.
(2) Armand, M.; Tarascon, J. M. *Nature* **2008**, *451*, 652.
(3) Lu, Y.-C.; Gasteiger, H. A.; Crumlin, E.; Robert McGuire, J.; Shao-Horn, Y. *J. Electrochem. Soc.* **2010**, *157*, A1016.
(4) Lu, Y.-C.; Gasteiger, H. A.; Parent, M. C.; Chiloyan, V.; Shao-Horn, Y. *Electrochem. Solid-State Lett.* **2010**, *13*, A69.
(5) Lu, Y.-C.; Gasteiger, H. A.; Shao-Horn, Y. *J. Am. Chem. Soc.* **2011**, *133*, 19048.
(6) Mitchell, R. R.; Gallant, B. M.; Thompson, C. V.; Shao-Horn, Y. *Energy Environ. Sci.* **2011**, *4*, 2952.
(7) Girishkumar, G.; McCloskey, B.; Luntz, A. C.; Swanson, S.; Wilcke, W. *J. Phys. Chem. Lett.* **2010**, *1*, 2193.
(8) Lu, Y.-C.; Xu, Z.; Gasteiger, H. A.; Chen, S.; Hamad-Schifferli, K.; Shao-Horn, Y. *J. Am. Chem. Soc.* **2010**, *132*, 12170.
(9) Ren, X.; Zhang, S. S.; Tran, D. T.; Read, J. *J. Mater. Chem.* **2011**, *21*, 10118.
(10) Débart, A.; Paterson, A. J.; Bao, J.; Bruce, P. G. *Angew. Chem., Int. Ed.* **2008**, *47*, 4521.
(11) Chen, Z.; Higgins, D.; Yu, A.; Zhang, L.; Zhang, J. *Energy Environ. Sci.* **2011**, *4*, 3167.
(12) Li, B.; Higgins, D. C.; Zhu, S.; Li, H.; Wang, H.; Ma, J.; Chen, Z. *Catal. Commun.* **2011**, *18*, 51.
(13) Zhang, L.; Kim, J.; Chen, H. M.; Nan, F.; Dudeck, K.; Liu, R.-S.; Botton, G. A.; Zhang, J. *J. Power Sources* **2011**, *196*, 9117.
(14) Bezerra, C. W. B.; Zhang, L.; Lee, K. C.; Liu, H. S.; Zhang, J. L.; Shi, Z.; Marques, A. L. B.; Marques, E. P.; Wu, S. H.; Zhang, J. J. *Electrochim. Acta* **2008**, *53*, 7703.
(15) Chen, Z.; Higgins, D.; Chen, Z. *Electrochim. Acta* **2010**, *55*, 4799.
(16) Chen, Z.; Higgins, D.; Chen, Z. *Carbon* **2010**, *48*, 3057.
(17) Chen, Z.; Higgins, D.; Tao, H.; Hsu, R. S.; Chen, Z. *J. Phys. Chem. C* **2009**, *113*, 21008.
(18) Choi, J.-Y.; Hsu, R. S.; Chen, Z. *J. Phys. Chem. C* **2010**, *114*, 8048.
(19) Lefevre, M.; Proietti, E.; Jaouen, F.; Dodelet, J. P. *Science* **2009**, *324*, 71.
(20) Li, H.; Liu, H.; Jong, Z. e.; Qu, W.; Geng, D.; Sun, X.; Wang, H. *Int. J. Hydrogen Energy* **2011**, *36*, 2258.
(21) Li, Y.; Wang, J.; Li, X.; Geng, D.; Li, R.; Sun, X. *Chem. Commun.* **2011**, *47*, 9438.
(22) Tsai, C.-W.; Tu, M.-H.; Chen, C.-J.; Hung, T.-F.; Liu, R.-S.; Liu, W.-R.; Lo, M.-Y.; Peng, Y.-M.; Zhang, L.; Zhang, J.; Shy, D.-S.; Xing, X.-K. *RSC Adv.* **2011**, *1*, 1349.
(23) Velazquez-Palenzuela, A.; Zhang, L.; Wang, L.; Cabot, P. L. s.; Brillas, E.; Tsay, K.; Zhang, J. *J. Phys. Chem. C* **2011**, *115*, 12929.
(24) Wu, G.; More, K. L.; Johnston, C. M.; Zelenay, P. *Science* **2011**, *332*, 443.
(25) Zhu, S.; Chen, Z.; Li, B.; Higgins, D.; Wang, H.; Li, H.; Chen, Z. *Electrochim. Acta* **2011**, *56*, 5080.
(26) Watanabe, T.; Ohtsuka, Y.; Nishiyama, Y. *Carbon* **1994**, *32*, 329.
(27) Arechederra, R. L.; Artyushkova, K.; Atanassov, P.; Minteer, S. D. *ACS Appl. Mater. Interfaces* **2010**, *2*, 3295.
(28) Matter, P. H.; Zhang, L.; Ozkan, U. S. *J. Catal.* **2006**, *239*, 83.
(29) Laoire, C. O.; Mukerjee, S.; Plichta, E. J.; Hendrickson, M. A.; Abraham, K. M. *J. Electrochem. Soc.* **2011**, *158*, A302.